Performance comparison of FeNiCo, FeNiCu and FeNiCoCu alloy particles as catalyst material for polymer electrolyte membrane fuel cells

Semih Ates[1] ⓘ · **Doğaç Tarı**[1] ⓘ · **Şerzat Safaltın**[1] ⓘ · **Burak Küçükelyas**[2] ⓘ ·
Duygu Yeşiltepe Özçelik[1] ⓘ · **Sebahattin Gürmen**[1] ⓘ

Abstract

Fuel cells are using for electric production via redox reactions where catalyst material are used for increasing sluggish rates of reactions. Polymer electrolyte membrane fuel cells are the most promising types for daily life usage. Platinum is the most known catalyst material and it leads to high prices of fuel cell. Thus, new materials should be innovated instead of noble catalyst materials. In this study, FeNiCo, FeNiCu, FeNiCoCu alloy particles were produced in both ultrasonic spray pyrolysis and mechanical alloying methods to innovate alternative catalyst materials. Products were characterized by XRD, SEM–EDS. Spherical particles which are very important for catalytic properties, were produced with ultrasonic spray pyrolysis method. Elemental weight percentage of particles were observed close to each other. First in the literature, gas flow test was applied to observe gas consumption rates and generate the initial parameters for simulation study which was done to compare catalytic performances of products and conventional Pt catalyst. Ultrasonic spray pyrolysis method provided more catalytic surface behaviors. FeNiCu and FeNiCoCu of this method were found as promising catalyst materials.

Keywords Alloy particles · Catalyst · Simulation · Fuel cell

Introduction

Fuel cells are the key technology of green energy production systems and solution for depleting petroleum based energy sources. They can be classified according to the components such as electrolyte. The most attractive output is the fuel cell's is low or zero emission. The efficiency of fuel cells can be improved to 60% of electricity. This provides the decrement at pollution for electrical energy conversion
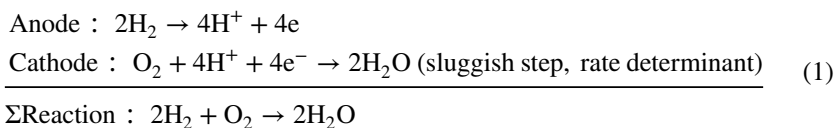
✉ Sebahattin Gürmen
  gurmen@itu.edu.tr

Extended author information available on the last page of the article

from thermal energy about > 90%. Fuel cell types are innovated for different usage parameters. Polymer electrolyte fuel cells (PEMFC) are very basic types because of their easy scale-up technology. Also, it generates high power density and low operating temperature which are made them the future power source for transportation/portable applications [1].

The main part of PEMFC is membrane electrode assembly that includes polymer electrolyte membrane, gas diffusion layer and catalytic layer. Catalytic layer contains electrode and electrolyte which is the basic cell for power generation. The outer parts are designed for homogenous gas (fuel) and output distribution. The main reaction which is occurred over catalyst is the oxygen reduction reaction (ORR). Thus, the catalyst material is the limiter for productivity and efficiency. There are three groups for PEMFC catalysts: Pt-based, Pt modified-based (Pt and metals such as Cr, Cu, Co or Ru), non-Pt based catalysts (i.e. non-noble metals, organometallics) [2]. As a consideration of effectivity, Pt is used as major catalyst material [3]. The over potential of half reaction is 500 – 600 mV with a platinum-based catalyst.

The overall chemical reactions that is occurred over catalyst of PEMFC are given in Eq. 1. The anode side is the power generator and cathode side is power depriver, because ORR is 100 times slower than hydrogen oxidation reaction (HOR) and electron usage. Also, cathode half reactions which provide different steps to carry out 4-electron direct and 2 electron indirect reduction are complicated because of strong O=O bond (498 kJ/mole) [4, 5]. However, ORR is not facile over Pt-catalyst thus over potentials are decreased with more catalyst usages. This is provided via increasing the surface area of catalyst as used as nano structures (2–6 nm for Pt) with 0.10 – 0.15 mg cm^{-2} anode loads [2, 6]. Even though Pt-based catalyst materials show the best catalytic performance for ORR, their high cost hinders the common applications of fuel cells [6, 7]. As a projection of United States Department of Energy (DOE, at 2007), the platinum-based catalyst layers have 56% coverage for the cost of fuel cell stack [7]. Also, 0.125 mg cm^{-2} is the 2017 target for Pt loading at anode + cathode that is ~ 0.4 mg cm^{-2} currently [8]. Hence, there is few ways should be considered in new technology: gas distribution optimization, operating temperature and inlet/outlet control, material innovation for membrane electrode assembly components. The sluggish ORR is the most challenging topic of fuel cells.

$$
\begin{aligned}
&\text{Anode}: \ 2H_2 \rightarrow 4H^+ + 4e \\
&\underline{\text{Cathode}: \ O_2 + 4H^+ + 4e^- \rightarrow 2H_2O \ (\text{sluggish step, rate determinant})} \\
&\Sigma\text{Reaction}: \ 2H_2 + O_2 \rightarrow 2H_2O
\end{aligned}
\tag{1}
$$

Non-precious metal catalysts are the most outstanding innovation for HOR and ORR of PEMFCs. There are several non-precious metal catalyst materials, such as transition metal based, iron based nanostructures, alloys, macrocyclic metal, carbon supported, electroconductive polymer based, metal nitrides, and carbon catalyst embedded compounds [6, 9]. The outstanding platinum-free catalyst is Se-modified Ru catalyst (RuSe$_x$/C) since it has 10 times higher ORR activity, electrooxidation protection of Ru and H$_2$O$_2$ formation suppression. However, same critical cost-supply problem occurs for Ru that regards to price and availability. Otherwise, metal

oxynitrides which is subgroup of IV and V elements, are promising ORR catalysts as a result of their high metal d-band concentration at the Fermi level. Another focused material are polymer-metal systems such as macrocycle metal compounds. The impressive behavior of this systems is being protective for harsh outputs of HOR and ORR. If in doubt non-noble material systems are not enough to fulfill all demands, they are superior for ORR that is the limiting parameter of a catalyst applications [10]. In contrast to two or three component conventional alloys, high entropy alloys shows impressive physicochemical and mechanical properties [11].

Medium and high entropy alloys (MEA & HEA) promising for mechanical applications and structural designs because of the lattice distortion how the different atomic sized components of material systems, but also they are advantageous for functional material designs because of tunable compositions. Except mechanics, other properties of MEAs and HEAs are still less undiscovered, especially for catalysis and energy applications. As is well known, the cocktail effect of HEA shows improved catalytic activity by tuning composition, geometry, structure and morphology. With the generation of more stable phase-separated materials or intermetallic compounds, the two components of binary alloy frequently exhibit a considerable immiscible gap which inhibits the continuous regulation of the composition ratio and also the catalytic activity. However, the occurrence of single stable solution phase from multiple elements generates the larger configuration entropy for HEAs [12]. Catalytic behaviors are driven from high surface area, optimum adsorption energetics, and d-band center theory which are can be achieved using subgroup of HEAs, transition metal HEAs [11, 13]. Moreover, HEA nanoparticles can have better electrocatalytic properties because of their large surface area, nanoscale effect and material utilization efficiency [11]. HEAs shows higher potential energy due to a lower energy barrier in catalytic reactions because of thermodynamically non-equilibrium state which is generated by lattice distortion effect. Also, compositional tuning and strain inducing provide HEAs to have adjusted catalytic selectivity that is observed by d-band center up/down shifting. Down shifting the d-band center via compressive lattice strain due to compositional design, generates weaker metal–molecule bindings [12]. The nano particle HEAs are used for thermal and electrochemical reactions, carbon dioxide reduction reaction, oxygen evolution (OER) and reduction reactions and hydrogen evolution reactions (HER), and others [14]. For example, FCC structured PtPdRhNi, PdCuPtNiCo, AlCuNiPt, and laves phased FeCoNiCrNb, CrMnFeCoNi (amorphous, FCC or BCC) are used for ORR, CoFeLaNiPt (amorphous phase) is used for OER and HER etc. [15].

Mainly, four $(O_2 + 4H^+ + 4e^- \rightarrow 2H_2O)$ or two $(O_2 + H_2O + 2e^- \rightarrow HO_2^- + OH^-)$ reactions are need to reduce oxygen to water. Rossmeisl and friends [16] generated a model to predict the surface adsorption energies of the ORR for different local compositions and calculated the surface adsorption energies of *OH and *O at (111) surface of IrPdPtRhRu HEA. As authors' study, $Ir_{0.102}Pd_{0.320}Pt_{0.093}Rh_{0.196}Ru_{0.289}$ was found to lower overpotential of Pt (111) as ~40 mV. The authors adjusted ligand effect which is the parameter of surface absorption behavior according to different local composition differences to obtain accurate prediction [15]. W. Chen and K. Li [17] plotted the overpotentials of metals at 10 mA/cm^2 and 1.0 M KOH and found that FeCoNiAlTi HEA had close overpotential property to noble metals. Löffler

et al. [18] produced CrMnFeCoNi as different particle sizes and crystal structures (BCC, FCC, and amorphous) that were produced complex solid solution nanoparticle sputtering over ionic liquids, to obtain the intrinsic ORR activities. 1.3 nm CrMnFeCoNi BCC compound (Mn,Fe $\leq$ 5 at%, Ni $\leq$ 10 at%, Co $\leq$ 20 at%, Cr $\leq$ 40 at%) showed highest activity and it was even higher than Pt nano particles. A. Aliyu and C. Srivastava FeNiCoCu MEA and FeNiCoCu MEA-graphene oxide composite coatings to observe electrochemical properties. Authors found that corrosion resistance decreased with lowering graphene amount [19].

It is needed to be done both experimental characterization and theoretical simulation for innovated catalyst materials, especially HEAs [13]. There is two case for simulation studies: modelling of ORR and adsorption properties of catalyst layers. However, multi-phase flows, charge-species and heat transfer mechanisms should be modelled mathematically as well as electrochemical reactions. Thus, this brings appliance of multi-physic approaches with related material properties [1]. Wang et al. [1] listed fuel cell governing and source terms conservation equations with frequently used electrochemical and transport properties which were used in this paper.

In this paper FeNiCo, FeNiCu, FeNiCoCu HEA alloy particles were produced with ultrasonic spray pyrolysis (USP) method that is studied our previous works (see [20–22]) and ball-mill (BM) methods to provide method-material-property trilemma. In addition to the XRD and SEM–EDS characterizations, first in the literature, gas flow tests were used to observe gas consumption rates to generate simulation parameters. The characterization results of the newly developed catalyst materials were compared with conventional catalyst material by examining the catalytic behaviors in an ideal fuel cell through simulation study.

Material and experiment

Material

Fe(NO$_3$)0.6H$_2$O, Ni(NO$_3$)$_2$.6H$_2$O, Co(NO$_3$)$_2$.6H$_2$O and Cu(NO$_3$)0.3H$_2$O (High purity, Merck, Germany) are used as raw materials for USP. Nitrate salts were dissolved with pure water to generate 0.2 M precursor solution. The reduction was done with H$_2$ (1 L/min) and system was purged with N$_2$ (1 /min). Also, Fe–Ni-Co–Cu metallic powders (particle size < 45 μm, min. 99.7% purity) were used at mechanical alloying, BM method. WC vials and WC balls (10 mm diameters) were used for BM. N-heptane was used as process control agent for preventing oxidation and excessive cold welding.

Experiment

In USP route, nitrate salts of components were dissolved with pure water according to 0.2 M concentration. Also, each solution was mixed for 15 min at 500 rpm to obtain homogenous precursor solution. The reduction was done at 800 °C with H$_2$ (1 L/min) which used reductant and aerosol droplet carrier. N$_2$ (1 L/min) was used at heating

(10 °C/min) and cooling (to room temperature) as purging gas. Precursor solution was turned to aerosol droplets via ultrasonic atomizer (Ramine Baghai Instrumentation) with 1.3 MHz. Circulating bath was used to stabilize the precursor temperature at 24 °C. Reduced particles were collected in collection chambers in ethanol (99.9%).

In mechanical alloying route, nanoparticles were produced with planetary ball-mill (Retsch™ PM 200) from metallic powders. Milling was done in WC vial and with WC balls (10 mm diameters). The medium to material ratio was 10:1, milling speed was 250 rpm and duration was 54 h. To avoid oxidation and excessive cold welding, n-heptane was used as process control agent.

Characterization

FeNiCo, FeNiCu and FeNiCoCu alloy particles were produced with ultrasonic spray pyrolysis and mechanical alloying method. The HEA phases was determined with XRD (model: Rigaku 200, 20°–90°, Cu*Ka*) and particle morphologies were observed with SEM–EDS (model: JEOL SEM–EDS). One point EDS measurement was done. XRD and SEM–EDS samples were prepared via dripping ethanol-produced particle suspension over silicon single crystal holder. After, these samples were dried under controlled atmosphere without heating to prevent extra agglomerations. Gas flow test (see Fig. 1) applied to obtain the initial values of simulation study and characterize the catalytic effect via gas inflow/outflow differences. Spent H_2, O_2 and formed H_2O were determined and integrated with simulation study via below equations (Eq. 2, 3, 4). V_{H_2} and V_{air} stands for the volumetric flow rates of H_2 and air, ϑ_{H_2} and ϑ_{air} denotes the measured volume of H_2 and air passing through per second, ρ_{H_2} and ρ_{air} are the gas densities, and MW_{H_2} and MW_{air} are the molecular weight of the gases. a_{H_2O} is activity of water and it was taken as 0.99 that regards to reference Pt catalyst. 21% of air was simply taken and accepted as fully consumed. V_{net} was used as total species flow and derived unreacted, excess H_2 volume in Eq. 3. Product ratio of H_2O was determined according to Eq. 4.

$$V_{H_2} = \frac{\vartheta_{H_2} * \rho_{H_2}}{60[\sec] * MW_{H_2}} \text{ and } V_{air} = \frac{\vartheta_{air} * \rho_{air}}{60[\sec] * MW_{air}} \left(O_2 \text{was taken as 21% of air.}\right)$$

$$(2)$$

$$V_{net} = V_{H_2} + V_{air} \text{ and } V_{excess,H_2} = V_{H_2} - 2 * V_{O_2} \tag{3}$$

Fig. 1 Schematic of gas flow test
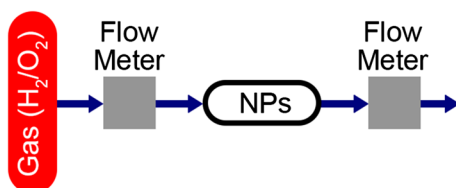
$$V_{H_2O} = 2 * V_{O_2} \text{ and } a_{H_2O} = \frac{V_{H_2O}}{V_{H_2O} + V_{excess,H_2}} \tag{4}$$

Finally, performance comparison was done between Pt and produced alloy particles with mathematical simulations. Conventional stacked PEMFC shape was used as geometry with dense mesh structure. The initial values were taken from characterization results and equations (see [1]) were used to calculate local current density for the HER and ORR, reacting flow in porous media, and inflow/outflow. Stationary solver was used to investigate catalytic behaviors of different alloy particles when flow rates reach constant regime.

Results and discussion

Structure and morphology

The crystal structure and phase of particles were investigated via XRD analysis ($\lambda_{CuK\alpha}$). The results of the XRD analysis are given in Fig. 2. The position of the diffraction peaks in the XRD pattern of both samples agree with data from literature for alloys in the Fe–Ni, Cu-Ni, Fe–Ni-Co, Fe–Ni-Co–Cu. Three main peaks at around 2θ of 43°, 51°, and 74° was corresponding to (111), (200), and (220) and FCC structure (JCPDS: 00–018-0646, 00–009-0205, [22–25]. Full width at half-maximum (FWHM) value for Scherrer equation (see [22, 26]) calculated at (111) plane to observe average crystallite size. Also, ultrasonic spray pyrolysis products showed higher crystallite sizes because of narrower peaks, lower FWHM values than mechanically alloyed particles.

SEM images are given in Fig. 3. It was emphasized at previous sections that the catalyst surface morphology, surface area and particle sizes are very
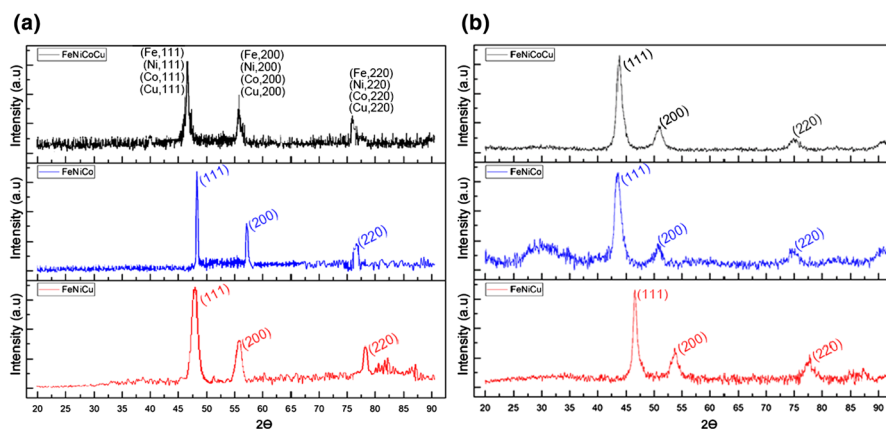
Fig. 2 XRD results of alloy particles (black: FeNiCoCu, blue: FeNiCo, red: FeNiCu) produced with **a** USP and **b** BM
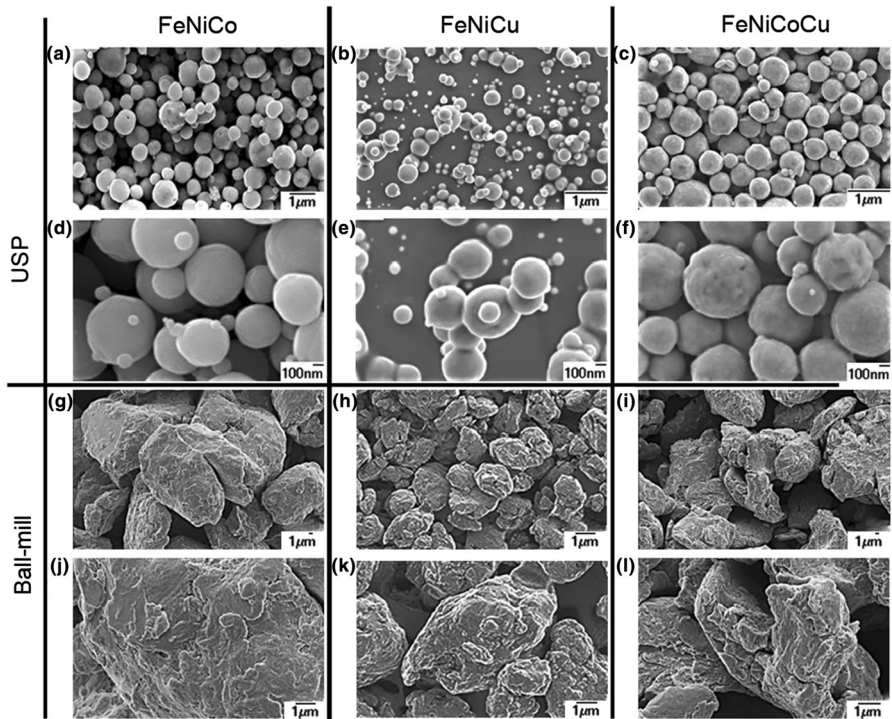
Fig. 3 SEM images of FeNiCo (**a**, **d**: USP; **g**, **j**: BM), FeNiCu (**b**, **e**: USP; **h**, **k**: BM), and FeNiCoCu (**c**, **j**: USP; **i**, **l**: BM) alloys

important for catalytic applications. Depending on the surface area of the catalyst, the amount of reactant and rate of the reaction may vary which will in turn effect the catalyst performance. USP products showed nearly homogenous size distribution and spherical particles. On the other hand, mechanical alloyed products had elliptical shapes and size distribution was heterogeneous. The particle sizes were measured with ImageJ open source software [27–30]. The resulted particle sizes of USP products were 248.85 nm, 203.14 nm, 385.77 nm for FeNiCo, FeNiCu, FeNiCoCu and BM products were 19.78 μm, 2.36 μm, 16.83 μm FeNiCo, FeNiCu, FeNiCoCu. The non-uniform particle distribution can cause partial load effect on electrodes. H_2/O_2 usages and H_2O formation will be localized because of the heterogeneous catalyst performance distribution over the electrode surface, and this situation will lead to non-uniform current density distribution. Also, with both production route, each elemental composition particle showed that the nanocrystallite grains were agglomerated.

Fe–Ni–Co–Cu weight percentages of corresponding particles are given in EDS results at Table 1. Both XRD and EDS results were clearly descriptive of near elemental distributions.

Table 1 EDS results of alloy particles

Production methods	Materials	Fe (wt.%)	Ni (wt.%)	Co (wt.%)	Cu (wt.%)
Ultrasonic spray pyrolysis (USP)	FeNiCo	29.37	32.78	37.85	–
	FeNiCu	27.88	37.48	–	34.64
	FeNiCoCu	23.74	25.02	25.84	25.4
Ball mill (BM)	FeNiCo	33.15	34.13	32.72	–
	FeNiCu	33.58	30.62	–	35.8
	FeNiCoCu	25.69	25.98	22.94	26.39

Performance analysis

Gas flow test was done to obtain gas consumption rates of produced alloy particles. $Rate = \frac{Rate_{specimen}}{Rate_{Pt}}$ function was used for comparison USP and BM alloy particles and conventional Pt nano particles. The rates were generated according to gas consumptions and the rate of Pt was taken as 1, $Rate_{Pt} = 1$ for idealizing the Pt catalyst performance. These ratios were used as reduced species in electrodes kinetics in simulation study. High catalytic activity of Cu, FeNiCu of USP and BM method had higher unstable usage results than other particles. However, other particles that produced with BM method showed periodic usages, especially for O_2 consumption. Also, H_2 usage of these particles followed the O_2 consumption trends. In USP produced particles, consumptions were unstable according to spherical shape of particles which causes the high catalytic activities. The H_2 consumption of USP products were observed to be high than those of O_2. Normalized mean gas consumption values ware used for each particle in accordance with gas flow meter results. The calculated average gas consumption rates of products are given in Table 2.

Catalytic performance results that were calculated via integration of gas flow test results and physical equations of PEMFC is given in Fig. 4.

According to compared results, products of USP had higher cell current density results than BM products. FeNiCu and FeNiCo alloy particles of USP method showed instability in between cut off cell voltages. Highest cell current density was observed for FeNiCoCu alloy particles of USP method because of the catalytic effect of Cu. The smaller Cu particles tends to have more corrosive properties, but

Table 2 Calculated consumption rates of products for simulation study

Production methods	Materials	Rate
Ultrasonic spray pyrolysis (USP)	FeNiCo	0.1764
	FeNiCu	0.2018
	FeNiCoCu	0.2235
Ball mill (BM)	FeNiCo	0.1482
	FeNiCu	0.1506
	FeNiCoCu	0.1718
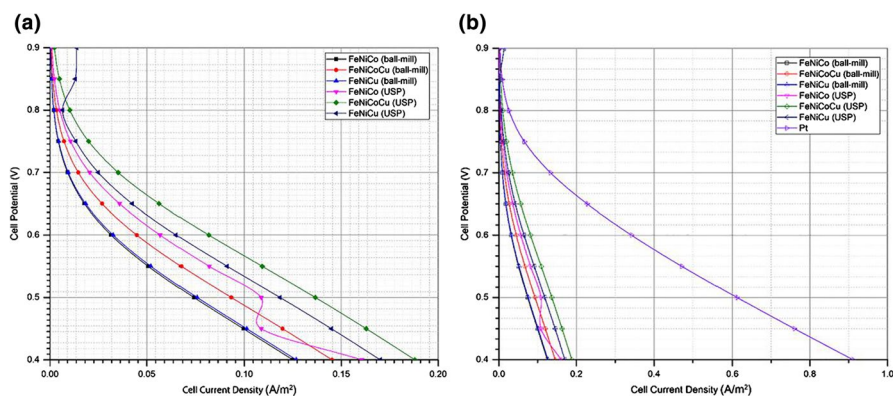
Fig. 4 Simulation result comparison of BM and USP products in each other (**a**) and conventional Pt (**b**)

togetherness of components gives the stability for FeNiCoCu. In both production routes, FeNiCo particles showed lowest efficiency. Considering the assumptions made in order to observe the catalytic effect in the simulation study, it can be seen that the FeNiCoCu or FeNiCu alloy particles of USP method can be alternative catalyst materials.

Conclusion

FeNiCo, FeNiCu and FeNiCoCu alloy particles were produced by mechanical alloying method from their metallic powders and ultrasonic spray pyrolysis method from their precursor solutions. Particles were characterized by XRD, SEM–EDS and gas flow tests. In micro-scale, USP products showed spherical shapes and homogenous particle size distribution, but elliptical shape and slight inhomogeneous particle size distribution was observed for BM products. Nanocrystalline particle grains were examined for both production route as shown in SEM results. EDS results shows that particles consist Fe–Ni-Co, Fe–Ni-Cu, and Fe–Ni-Co–Cu elements with nearly same weight distribution.

Ternary and quaternary alloys were produced with close atomic ratios with both USP and BM methods. Physical equations of PEMFC was integrated with gas flow test equations and simulation study was done to obtain catalytic performance comparison. FeNiCo or FeNiCu showed unstable performance but Cu increased the catalytic efficiency because of its high catalytic properties. On the other hand, stable and highest catalytic performance was observed for FeNiCoCu. According to comparison of Pt catalyst, FeNiCoCu alloy particles of USP route was found as promising catalyst material to lower prices of PEMFC that contains Pt catalyst.

Authors' contributions SA, DT, ŞS, BK and SG conceived and planned experiments. SA, DT and ŞS planned and carried out the simulations and gas flow test. BK contributed to mechanical alloying technique. ŞS, DYÖ and SG contributed to the interpretation of the results. SA and DT took the lead in writing the manuscript. Also, the introduction part was written by SA. All authors provided critical feedback and helped shape the research, analysis and manuscript.

Data Availability Data sharing is not applicable to this article as no new data were created or analyzed in this study.

Declarations

Conflict of interest The authors have no conflict of interest to declare. Also, no funding was received to assist with the preparation of this manuscript.

References

1. Wang Y, Chen KS, Mishler J, Cho SC, Adroher XC (2011) A review of polymer electrolyte membrane fuel cells: Technology, applications, and needs on fundamental research. Appl Energy 88:981–1007
2. Majlan EH, Rohendi D, Daud WRW, Husaini T, Haque MA (2018) Electrode for proton exchange membrane fuel cells: A review. Renew Sustain Energy Rev 89:117–134
3. Napporn TW, Karpenko-Jereb L, Pichler B, Hacker V (2018) Polymer electrolyte fuel cells. Fuel Cells Hydrog From Fundam to Appl Res. 63–89. https://doi.org/10.1016/B978-0-12-811459-9.00004-9
4. Song C, Zhang J (2008) Electrocatalytic oxygen reduction reaction. In: Zhang J (ed) PEM Fuel Cell Electrocatalysts and Catalyst Layers. Springer, London
5. Gewirth AA, Thorum MS (2010) Electroreduction of dioxygen for fuel-cell applications: Materials and challenges. Inorg Chem 49:3557–3566
6. Banham D, Ye S, Pei K, Ozaki JI, Kishimoto T, Imashiro Y (2015) A review of the stability and durability of non-precious metal catalysts for the oxygen reduction reaction in proton exchange membrane fuel cells. J Power Sources 285:334–348
7. Nie Y, Li L, Wei Z (2015) Recent advancements in Pt and Pt-free catalysts for oxygen reduction reaction. Chem Soc Rev 44:2168–2201
8. Sui S, Wang X, Zhou X, Su Y, Riffat S, Liu C (2017) A comprehensive review of Pt electrocatalysts for the oxygen reduction reaction: Nanostructure, activity, mechanism and carbon support in PEM fuel cells. J Mater Chem A 5:1808–1825
9. Chakraborty M (2017) Cost effective non precious metal catalyst for application in fuel cells. Int J Eng Tech Res 7:57–60
10. Kramm UI, Bogdanoff P, Fiechter S (2012) Polymer Electrolyte Membrane Fuel Cells (PEM-FC) and Non-noble Metal Catalysts for Oxygen Reduction. In: Meyers RA (ed) Encycl. Sustain. Sci. Technol, Springer, New York New York, NY, pp 8265–8307
11. Tomboc GM, Kwon T, Joo J, Lee K (2020) High entropy alloy electrocatalysts: a critical assessment of fabrication and performance. J Mater Chem A 8:14844–14862
12. Xin Y, Li S, Qian Y, Zhu W, Yuan H, Jiang P, Guo R, Wang L (2020) High-entropy alloys as a platform for catalysis: progress, challenges, and opportunities. ACS Catal 10:11280–11306
13. Kumar Katiyar N, Biswas K, Yeh J-W, Sharma S, Sekhar Tiwary C (2021) A perspective on the catalysis using the high entropy alloys. Nano Energy 88:106261
14. Zheng H, Luo G, Zhang A, Lu X, He L (2021) The synthesis and catalytic applications of nanosized high-entropy alloys. ChemCatChem 13:806–817
15. Sun Y, Dai S (2021) High-entropy materials for catalysis: A new frontier. Sci Adv 7:eabg1600

16. Batchelor TAA, Pedersen JK, Winther SH, Castelli IE, Jacobsen KW, Rossmeisl J (2019) High-entropy alloys as a discovery platform for electrocatalysis. Joule 3:834–845
17. Li K, Chen W (2021) Recent progress in high-entropy alloys for catalysts: synthesis, applications, and prospects. Mater Today Energy 20:100638
18. Manjón AG, Löffler T, Meischein M, Meyer H, Lim J, Strotkötter V, Schuhmann W, Ludwig A, Scheu C (2020) Sputter deposition of highly active complex solid solution electrocatalysts into an ionic liquid library: effect of structure and composition on oxygen reduction activity. Nanoscale 12:23570–23577
19. Aliyu A, Srivastava C (2021) Microstructure and electrochemical properties of FeNiCoCu medium entropy alloy-graphene oxide composite coatings. J Alloys Compd 864:158851
20. Gurmen S, Ebin B, Stopić S, Friedrich B (2009) Nanocrystalline spherical iron-nickel (Fe-Ni) alloy particles prepared by ultrasonic spray pyrolysis and hydrogen reduction (USP-HR). J Alloys Compd 480:529–533
21. Gurmen S, Guven A, Ebin B, Stopić S, Friedrich B (2009) Synthesis of nano-crystalline spherical cobalt–iron (Co–Fe) alloy particles by ultrasonic spray pyrolysis and hydrogen reduction. J Alloys Compd 481:600–604
22. Toparli C, Ebin B, Gürmen S (2017) Synthesis, structural and magnetic characterization of soft magnetic nanocrystalline ternary FeNiCo particles. J Magn Magn Mater 423:133–139
23. Chen XP, Sun HF, Chen D, Wang LX, Liu Q (2016) On recrystallization texture and magnetic property of Cu-Ni alloys. Mater Charact 121:149–156
24. Zheng R, Chen J, Xiao W, Ma C (2016) Microstructure and tensile properties of nanocrystalline (FeNiCoCu)1-xTixAlx high entropy alloys processed by high pressure torsion. Intermetallics 74:38–45
25. Yang D-S, Oh K, Na W, Kim N, Yoo Y-G, Min S-G, Yu S-C (2007) X-Ray Absorption Fine Structure Study for Fe60Ni40 Alloy. AIP Conf Proc AIP 882:460–462
26. Mahshid S, Askari M, Sasani Ghamsari M, Afshar N, Lahuti S (2009) Mixed-phase TiO2 nanoparticles preparation using sol-gel method. J Alloys Compd 478:586–589
27. Benhammada A, Trache D, Kesraoui M, Chelouche S (2020) Hydrothermal synthesis of hematite nanoparticles decorated on carbon mesospheres and their synergetic action on the thermal decomposition of nitrocellulose. Nanomaterials. https://doi.org/10.3390/nano10050968
28. Kumari R, Rana N (2015) Particle Size and Shape Analysis using Imagej with Customized Tools for Segmentation of Particles. Int J Eng Res V4:247–250
29. Igathinathane C, Pordesimo LO, Columbus EP, Batchelor WD, Methuku SR (2008) Shape identification and particles size distribution from basic shape parameters using ImageJ. Comput Electron Agric 63:168–182
30. Abràmoff MD, Magalhães PJ, Ram SJ (2004) Image processing with imageJ Biophotonics Int 11:36–41

Authors and Affiliations

Semih Ates[1] · **Doğaç Tarı[1]** · **Şerzat Safaltın[1]** · **Burak Küçükelyas[2]** · **Duygu Yeşiltepe Özçelik[1]** · **Sebahattin Gürmen[1]**

Semih Ates
atessem@itu.edu.tr

Doğaç Tarı
dogactari@gmail.com

Şerzat Safaltın
safaltin@itu.edu.tr

Burak Küçükelyas
burak.kucukelyas@itu.edu.tr

Duygu Yeşiltepe Özçelik
yesiltepe15@itu.edu.tr

[1]   Department of Metallurgical and Materials Engineering, Istanbul Technical University,
      Istanbul 34469, Turkey

[2]   Department of Metallurgical and Materials Engineering, Bursa Technical University,
      Bursa 16310, Turkey